Analytical Biochemistry 593 (2020) 113580

Contents lists available at ScienceDirect

Analytical Biochemistry

journal homepage: www.elsevier.com/locate/yabio

The impact of different human IgG capture molecules on the kinetics analysis of antibody-antigen interaction

Vishal Kamat[a,*], Ashique Rafique[a], Tammy Huang[b], Olav Olsen[b], William Olson[b]

[a] Biomolecular HTS Center, Therapeutic Proteins, Regeneron Pharmaceuticals, Tarrytown, NY, USA
[b] Therapeutic Proteins, Regeneron Pharmaceuticals, Tarrytown, NY, USA

ARTICLE INFO

Keywords:
Label-free optical biosensor
SPR
KinExA
Monoclonal antibody
Anti-human Fc
Binding kinetics
Capture kinetics
Capture antibody

ABSTRACT

Surface plasmon resonance (SPR) is a well-established method to characterize biomolecular interactions and is widely used in drug discovery and development. Here, we demonstrate that capture surfaces profoundly impact the binding kinetics parameters that are measured for antibody-antigen interactions. Six unique antibody-antigen interactions were characterized using eight different anti-human IgG capture surfaces. The antigen binding affinities for six different human monoclonal antibodies (hmAbs) captured using three different goat anti-human Fc (AHC) polyclonal antibody (pAb) surfaces were in reasonable agreement (3-7-fold weaker) with those measured by kinetic exclusion assay (KinExA). In contrast, up to 81, 32, 489, 2826, and 219-fold weaker antigen binding affinities were measured using mouse AHC mAb, Protein G, Protein A, Protein A/G, and Protein L surfaces, respectively. Protein A, Protein A/G and Protein G interacted with the Fab of hmAbs, possibly affecting antigen binding to hmAbs captured over these surfaces. Additional studies revealed that mouse AHC mAb binds hmAbs with a weak affinity (5.5–36.3 nM) and $t_{½}$ values of 1.4–3.3min, compared to the sub-nanomolar affinities of the goat AHC pAbs. These results emphasize the value of measuring binding kinetics of the capture molecule before immobilizing them onto the sensor surface to perform capture kinetics assays on label-free biosensors.

1. Introduction

Therapeutic monoclonal antibodies (mAbs) represent the leading product class within the biopharmaceutical market [1–3]. Numerous biophysical, biochemical, *in-vitro* functional and *in-vivo* assays are performed before selecting a lead therapeutic mAb. Amongst the various properties evaluated, the kinetics of mAb binding to its target antigen (Ag) is one of the important parameters used to select a clinical candidate. Different real-time, label-free (RT-LF) optical biosensors allow for the rapid and reproducible measurement of association rate (k_a), dissociation rate (k_d), and equilibrium dissociation constant (K_D) of biomolecular interactions and hence are widely used to characterize mAb-Ag interactions [4–6]. In such assays, one binding partner is immobilized onto the sensor surface (referred to as a ligand). This is achieved either by covalently linking the ligand onto the sensor surface (direct immobilization assay) or by capturing the ligand via a tag specific capture molecule that is covalently immobilized on the sensor surface (capture kinetics assay). Although researchers have adopted direct immobilization assays to characterize mAb-Ag interactions, successful application of this technique requires overcoming several challenges, such as: (i) conjugation reactions typically result in a random, multi-oriented mAb surface, which may affect Ag binding activity, (ii) stability of the immobilized mAb following prolonged exposure to experimental conditions used for surface regeneration and analysis temperature, (iii) time consuming optimization of regeneration conditions for each mAb surface. A major advantage of the capture kinetics assay is that mAbs are typically captured via their Fc domains, which should not sterically hinder Ag binding to the variable region, allowing reliable characterization of mAb-Ag interactions. The capture kinetics assay provides additional advantages such as: (i) allows for the capture of unpurified mAb from conditioned media (CM); (ii) retains the binding activity of captured mAb, especially while performing kinetics assays at higher temperatures (such as 37°C), as the mAb captured at the beginning of each cycle is exposed to higher temperatures only for a short period; (iii) allows for rapid optimization of the mAb capture density; and (iv) requires shorter assay development time, as surface regeneration at the end of each cycle removes both Ag bound and unbound mAb and is independent of the Ag binding profile of the captured mAb. These favorable characteristics have made the capture kinetics assay the preferred screening tool for rapid measurement of k_a,

* Corresponding author.
E-mail address: vishal.kamat@regeneron.com (V. Kamat).

https://doi.org/10.1016/j.ab.2020.113580
Received 3 November 2019; Accepted 6 January 2020
Available online 10 January 2020

Abbreviations

real-time, label-free (RT-LF)
monoclonal antibody (mAb)
anti-human Fc (AHC)
anti-human IgG (AHG)
association rate (k_a)
dissociation rate (k_d)
equilibrium dissociation constant (K_D)
antigen binding fragment of mAb (Fab)
polyclonal antibody (pAb)
surface plasmon resonance (SPR)
kinetic exclusion assay (KinExA)
constant binding partner (CBP)
polyclonal antibody (pAb)
antigen (Ag)
human monoclonal antibody (hmAb)
human IgG (hIgG)
variable kappa domain (VK)
variable lambda domain (VL)
isoelectric point (pI)
fragment crystallizable (Fc)
constant region (CH)
resonance units (RU)
conditioned media (CM)
iminodiacetic acid (IDA)

k_d, and K_D values of mAbs.

The current study was undertaken after we unexpectedly found that capturing a human mAb (hmAb) over a mouse anti-human Fc (AHC) mAb immobilized surface resulted in the measurement of a 10-fold faster dissociation rate compared to capturing the same hmAb on a goat anti-human Fcγ specific polyclonal antibody (pAb) surface on a surface plasmon resonance (SPR) biosensor (data not shown). To understand the source of this discrepancy, we performed a series of systematic and detailed binding kinetics studies using SPR and solution equilibrium based kinetic exclusion assay (KinExA). Two additional commercially available goat AHC pAbs and four non-antibody anti-human IgG (AHG) molecules – Protein A, Protein A/G, Protein G, and Protein L, which are commonly used by label-free users were also included to perform capture kinetics assay on the SPR biosensor [4,7–13]. The ability of these eight capture molecules to stably capture hmAbs and their utility to measure the kinetics of hmAb-Ag interactions were assessed.

A total of six different hmAb-Ag interactions were characterized in this study via SPR using four AHC and four AHG capture surfaces and KinExA. The hmAbs were selected based on their picomolar binding affinities to their respective Ags, germline diversity and the molecular weights of the Ags. The details of the hmAbs and Ags with the hmAb germline and the predicted pI values of the hmAbs and Ags (based on their amino acid sequence) are provided in Table 1. The hmAb-1 uses the VH4 germline, while the rest of the hmAbs are from the VH3 family. The hmAb-2 and hmAb-4 uses the same VH3-33 germline but have different VK gene usage.

The discrepancies in the k_a, k_d, and K_D values for hmAb-Ag interactions determined using the SPR biosensor were attributed to the different AHC and AHG capture surfaces. Additional SPR binding studies were performed to understand the disagreement in the kinetics values measured using mouse AHC mAb, Protein A, Protein G, and Protein A/G capture surfaces. This is the first study that describes the importance of measuring the true 1:1 binding kinetics of the capture molecule before immobilizing it on the sensor surface at high density to perform capture kinetics analysis on label-free optical biosensors.

2. Materials & methods

Reagents: N-(3-dimethylaminopropyl)-N-ethylcarbodiimide (EDC) N-hydroxysuccinimide (NHS), ethanolamine–HCl (Catalog# BR100633), CM5 sensor chip (Catalog# BR100530) and mouse AHC mAb (Catalog# BR100839) were purchased from GE Healthcare. Different AHC specific pAbs were purchased from Jackson ImmunoResearch (subsequently referred as goat AHC pAb-1), MP Biomedicals (subsequently referred as goat AHC pAb-2), and Southern Biotech (subsequently referred as goat AHC pAb-3) while the four AHG molecules; Protein A, Protein G, Protein A/G, and Protein L were purchased from ThermoFisher Scientific Pierce. Details of all the capture molecules used in this study are provided in Supplementary Table 1. HEPES (Teknova, Catalog# H1035), NaCl (Gibco, Catalog# 24740-011), EDTA (BDH, Catalog# BDH8730-1) and Tween-20® (Bio-Rad, Catalog# 161-0781) were used to prepare running buffer.

All hmAbs used in this study were expressed either with a wild-type human IgG1 constant domain or with a human IgG4 constant domain containing a serine to proline amino acid substitution (S228P) in the hinge region ($IgG4^P$) that reconstructs the human IgG1 hinge sequence (CPPC) to promote stabilization of disulfide bonds between the two heavy chains. The Ags are monomeric ectodomains of single transmembrane type-I receptors recombinantly expressed with a C-terminal hexahistidine (6xHis) tag. A total of six Ags were characterized in this study and their molecular weights were calculated based on their amino acid sequence (shown in Table 1). All the hmAbs, Ag binding fragment of hmAbs (hFabs) and Ags were recombinantly expressed using stable Chinese hamster ovary (CHO) cell lines. The hmAbs were purified using Protein A resin affinity column while the Ags were purified by IMAC affinity column; using either zinc charged iminodiacetic acid (IDA) resin or cobalt charged TALON resin. The reagents were further purified by size exclusion chromatography and their concentrations were determined by measuring their absorbances at 280 nm and their predicted extinction coefficients (based on their amino acid sequence) and stored at −80°C until used.

Table 1
Molecular properties of the hmAbs and their respective Ags included in the study.

hmAb Details					Ag Details		
hmAb	hmAb Isotype	VK Germline	VL Germline	Predicted pI	Ag	Ag M.W.	Predicted pI
hmAb-1	$IgG4^P$	IGHV4-39	IGKV3-20	8.96	Ag-1	14.8	5.29
hmAb-2	IgG1	IGHV3-33	IGKV1-17	9.39	Ag-2	17.9	5.90
hmAb-3	IgG1	IGHV3-48	IGKV3-11	9.14	Ag-3	27.7	5.59
hmAb-4	IgG1	IGHV3-33	IGKV3-11	9.11	Ag-4	57.8	5.92
hmAb-5	$IgG4^P$	IGHV3-20	IGKV1-9	6.30	Ag-5	72	6.30
hmAb-6	$IgG4^P$	IGHV3-23	IGKV1-33	6.08	Ag-6	73.1	5.81

2.1. Instrumentation

The solution based binding equilibrium experiments were performed using KinExA 3200 with the autosampler (Sapidyne Instruments, Boise, ID, USA) while real-time binding studies were performed on SPR based Biacore 3000, Biacore 4000 and Biacore 8k optical biosensors (GE Healthcare).

2.2. Binding equilibrium and kinetics measurements on KinExA

All the KinExA studies were performed at room temperature (~22°C) and samples were prepared in filtered buffer containing 10 mM HEPES, 150 mM NaCl, 3 mM EDTA, 0.05% Tween-20®, pH 7.4 (HBS-ET), supplemented with 1 mg/mL BSA and 0.02% sodium azide (subsequently referred as "KinExA buffer"). The Ag was first immobilized onto the azlactone beads (Sapidyne Instruments, Catalog# 444110) at room temperature following manufacturer's protocol. Briefly, 10 μg of Ag diluted in 1 mL of coating solution (50 mM sodium carbonate, 0.5 M sodium citrate, pH 9.0) was directly added to the premeasured azlactone activated beads and rocked for 2 h. The beads were later washed twice with blocking buffer (1 M Tris buffer containing 10 mg/mL BSA, pH 8.0) by gentle centrifugation and later rocked for 1 h in 1 mL of blocking buffer. The coupled beads were later washed twice in KinExA buffer and finally stored in the same buffer at 4°C.

The sample injection volumes were varied depending upon the hmAb and hFab tested, while the samples were injected at a flow rate of less than 0.7 mL/min. For binding equilibrium experiments, fixed

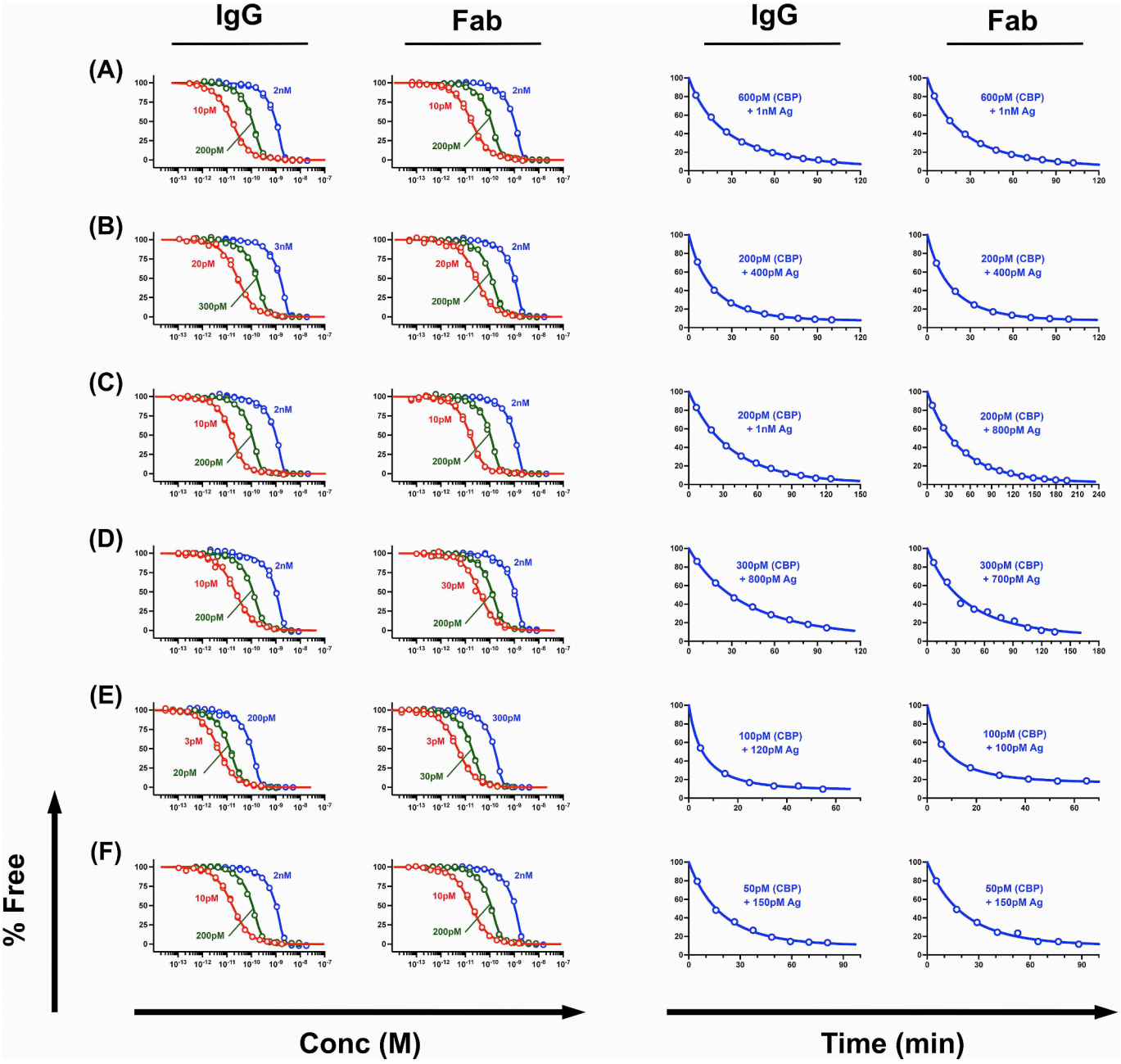

Fig. 1. KinExA equilibrium titration curves for six hmAbs and their respective hFabs. The left two panels show three-curve analysis performed using fixed concentrations of hmAbs or hFabs incubated with 12–16 point two-fold serial dilutions of (A) Ag-1, (B) Ag-2, (C) Ag-3, (D) Ag-4, (E) Ag-5, and (F) Ag-6. The fixed concentrations of hmAbs and hFabs used to generate the titration curves are also provided. The "direct method" was used to measure the k_a of hmAbs and hFabs; the right two panels show representative curves from at least four independent experiments. The CBP and Ag concentrations used to generate the curves are provided in the figure.

concentration of hmAb or hFab (also referred as the constant binding partner – CBP) was incubated with two-fold serial dilutions of Ag. Supplementary Table 2 provides CBP and Ag concentrations used to generate the three titration curves. The samples containing CBP and Ag were equilibrated for at least 36 h under constant rocking before measuring the unbound hmAb or hFab on KinExA 3200. The hmAb or hFab bound to the Ag coated azlactone beads was detected using the Alexa647-labeled affinipure goat anti-human IgG (H + L) (Jackson ImmunoResearch, Catalog# 109-605-088). The concentration, volume, and flow rate of the secondary antibody were varied to produce a signal of less than 1.0 V.

The K_D-controlled curve was generated by selecting the CBP concentration approximately equal to the K_D of the hmAb-Ag interaction; while the CBP concentration was fixed at 70-200-fold above the K_D to generate the receptor-controlled curve. A third binding equilibrium curve (referred as the intermediate curve) was also generated by selecting CBP concentration approximately 7-20-fold above the K_D value. The binding affinity of hmAb-Ag or hFab-Ag interactions was determined by first fitting the individual titration curves using the equilibrium binding analysis method using the "constant partner" as the analysis concentration reference. All three titration curves were later simultaneously fitted using the n-curve analysis in the KinExA software

Table 2
KinExA and SPR binding kinetics measurements performed on six hmAbs and hFabs.

Antigen	Analysis Method	Antibody Format	Capture Surface	k_a ($M^{-1}s^{-1}$)	k_d (s^{-1})	K_D (M)	% Antigen Activity
Ag-1 (14.8kD)	KinExA	Fab	N/A	7.59 (0.34) x 10^5	9.60 (0.43) x 10^{-6}	1.27 (0.99–1.61) x 10^{-11}	102.42 (92.13–110.20)
		IgG		8.07 (0.91) x 10^5	5.37 (0.06) x 10^{-6}	6.66 (4.41–9.80) x 10^{-12}	96.63 (86.32–107.82)
	SPR Capture Kinetics		Mouse AHC mAb	3.73 (0.41) x 10^5	1.98 (0.27) x 10^{-4}	5.37 (1.06) x 10^{-10}	N/A
			Goat AHC pAb-1	3.79 (0.16) x 10^5	1.5 (0.26) x 10^{-5}	3.95 (0.64) x 10^{-11}	
			Goat AHC pAb-2	4.26 (1.02) x 10^5	1.28 (0.17) x 10^{-5}	3.10 (0.75) x 10^{-11}	
			Goat AHC pAb-3	3.69 (0.11) x 10^5	1.40 (0.10) x 10^{-5}	3.8 (0.36) x 10^{-11}	
			Protein A	4.25 (0.29) x 10^5	1.02 (0.03) x 10^{-4}	2.42 (0.24) x 10^{-10}	
			Protein A/G	2.67 (0.29) x 10^5	6.64 (1.67) x 10^{-5}	2.56 (0.88) x 10^{-10}	
			Protein G	3.15 (0.28) x 10^5	4.13 (0.32) x 10^{-5}	1.31 (0.20) x 10^{-10}	
			Protein L	Poor baseline stability of captured hmAb			
Ag-2 (17.9kD)	KinExA	Fab	N/A	2.38 (0.19) x 10^6	4.28 (0.33) x 10^{-5}	1.80 (1.34–2.47) x 10^{-11}	83.91 (74.36–83.91)
		IgG		2.40 (0.20) x 10^6	4.13 (0.41) x 10^{-5}	1.75 (1.28–2.35) x 10^{-11}	92.31 (83.81–101.11)
	SPR Capture Kinetics		Mouse AHC mAb	5.57 (0.20) x 10^5	2.44 (0.72) x 10^{-4}	4.42 (1.44) x 10^{-10}	N/A
			Goat AHC pAb-1	7.99 (1.48) x 10^5	6.82 (0.14) x 10^{-5}	8.75 (1.79) x 10^{-11}	
			Goat AHC pAb-2	7.31 (0.98) x 10^5	7.00 (0.77) x 10^{-5}	9.69 (1.49) x 10^{-11}	
			Goat AHC pAb-3	8.90 (1.56) x 10^5	7.45 (0.54) x 10^{-5}	8.54 (1.70) x 10^{-11}	
			Protein A	1.14 (0.03) x 10^5	1.16 (0.01) x 10^{-4}	1.01 (0.01) x 10^{-9}	
			Protein A/G	4.20 (0.22) x 10^4	1.19 (0.05) x 10^{-4}	2.83 (0.06) x 10^{-9}	
			Protein G	4.16 (0.05) x 10^5	1.38 (0.22) x 10^{-4}	3.31 (0.05) x 10^{-10}	
			Protein L	3.97 (0.21) x 10^5	1.52 (0.13) x 10^{-3}	3.83 (0.13) x 10^{-9}	
Ag-3 (27.7kD)	KinExA	Fab	N/A	4.67 (0.26) x 10^5	5.21 (0.29) x 10^{-6}	1.11 (0.74–1.62) x 10^{-11}	103.19 (89.14–118.33)
		IgG		4.79 (0.34) x 10^5	4.91 (0.34) x 10^{-6}	1.02 (0.74–1.39) x 10^{-11}	102.69 (91.35–110.64)
	SPR Capture Kinetics		Mouse AHC mAb	2.24 (0.05) x 10^5	7.78 (1.73) x 10^{-5}	3.48 (0.80) x 10^{-10}	
			Goat AHC pAb-1	2.02 (0.08) x 10^5	1.06 (0.20) x 10^{-5}	5.24 (0.81) x 10^{-11}	
			Goat AHC pAb-2	1.97 (0.11) x 10^5	1.49 (0.30) x 10^{-5}	7.63 (1.66) x 10^{-11}	
			Goat AHC pAb-3	1.95 (0.20) x 10^5	9.50 (3.47) x 10^{-6}	4.78 (1.38) x 10^{-11}	
			Protein A	1.80 (0.07) x 10^4	6.68 (0.84) x 10^{-5}	3.72 (0.57) x 10^{-9}	
			Protein A/G	9.65 (1.50) x 10^3	1.32 (0.34) x 10^{-5}	1.41 (0.54) x 10^{-9}	
			Protein G	1.65 (0.50) x 10^5	5.12 (0.46) x 10^{-5}	3.26 (0.82) x 10^{-10}	
			Protein L	Poor baseline stability of captured hmAb			
Ag-4 (57.8kD)	KinExA	Fab	N/A	5.24 (0.91) x 10^5	1.15 (0.20) x 10^{-5}	2.20 (1.32–4.50) x 10^{-11}	41.29 (34.85–48.98)
		IgG		5.30 (0.82) x 10^5	9.13 (1.41) x 10^{-6}	1.72 (1.19–2.59) x 10^{-11}	42.69 (36.61–49.87)
	SPR Capture Kinetics		Mouse AHC mAb	2.35 (0.16) x 10^5	5.91 (1.33) x 10^{-5}	2.54 (0.75) x 10^{-10}	N/A
			Goat AHC pAb-1	2.35 (0.28) x 10^5	1.35 (0.28) x 10^{-5}	5.66 (1.03) x 10^{-11}	
			Goat AHC pAb-2	2.26 (0.36) x 10^5	1.35 (0.31) x 10^{-5}	5.99 (0.56) x 10^{-11}	
			Goat AHC pAb-3	2.37 (0.32) x 10^5	1.28 (0.24) x 10^{-5}	5.33 (0.50) x 10^{-11}	
			Protein A	2.22 (0.24) x 10^5	4.79 (0.50) x 10^{-5}	2.15 (0.06) x 10^{-10}	
			Protein A/G	1.53 (0.29) x 10^5	5.20 (0.80) x 10^{-5}	3.41 (0.20) x 10^{-10}	
			Protein G	1.55 (0.20) x 10^5	3.22 (0.39) x 10^{-5}	2.09 (0.11) x 10^{-10}	
			Protein L	Poor baseline stability of captured hmAb			
Ag-5 (72kD)	KinExA	Fab	N/A	2.57 (0.29) x 10^7	8.60 (0.95) x 10^{-5}	3.35 (2.71–4.29) x 10^{-12}	101.55 (93.61–110.27)
		IgG		2.53 (0.16) x 10^7	7.63 (0.05) x 10^{-5}	3.01 (2.29–3.92) x 10^{-12}	100.96 (90.67–113.11)
	SPR Capture Kinetics		Mouse AHC mAb	6.00 (0.59) x 10^6	1.66 (0.19) x 10^{-4}	2.81 (0.60) x 10^{-11}	
			Goat AHC pAb-1	6.01 (1.02) x 10^6	1.09 (0.09) x 10^{-4}	1.87 (0.49) x 10^{-11}	
			Goat AHC pAb-2	6.97 (1.17) x 10^6	1.06 (0.09) x 10^{-4}	1.54 (0.15) x 10^{-11}	
			Goat AHC pAb-3	6.12 (1.15) x 10^6	1.04 (0.03) x 10^{-4}	1.73 (0.29) x 10^{-11}	
			Protein A	1.96 (0.75) x 10^6	2.84 (0.91) x 10^{-3}	1.47 (0.16) x 10^{-9}	
			Protein A/G	7.50 (0.31) x 10^5	6.40 (1.09) x 10^{-3}	8.51 (1.16) x 10^{-9}	
			Protein G	4.54 (1.63) x 10^6	1.58 (0.08) x 10^{-4}	3.78 (1.27) x 10^{-11}	
			Protein L	3.27 (0.77) x 10^6	2.79 (0.14) x 10^{-4}	8.93 (2.60) x 10^{-11}	
Ag-6 (73.1kD)	KinExA	Fab	N/A	5.23 (0.20) x 10^6	6.28 (0.24) x 10^{-5}	1.20 (0.97–1.49) x 10^{-11}	76.73 (70.83–83.94)
		IgG		4.12 (0.55) x 10^6	4.86 (0.65) x 10^{-5}	1.18 (0.88–1.56) x 10^{-11}	88.00 (78.5–97.98)
	SPR Capture Kinetics		Mouse AHC mAb	2.31 (1.25) x 10^6	1.49 (0.27) x 10^{-4}	7.18 (2.10) x 10^{-11}	N/A
			Goat AHC pAb-1	2.50 (0.55) x 10^6	8.76 (1.12) x 10^{-5}	3.62 (0.88) x 10^{-11}	
			Goat AHC pAb-2	2.20 (0.76) x 10^6	7.75 (0.68) x 10^{-5}	3.75 (1.04) x 10^{-11}	
			Goat AHC pAb-3	2.53 (0.71) x 10^6	8.65 (0.12) x 10^{-5}	3.58 (0.92) x 10^{-11}	
			Protein A	4.60 (0.41) x 10^5	7.00 (1.67) x 10^{-5}	1.51 (0.23) x 10^{-10}	
			Protein A/G	2.84 (0.22) x 10^5	6.48 (0.70) x 10^{-5}	2.31 (0.43) x 10^{-10}	
			Protein G	1.14 (0.33) x 10^6	1.47 (0.22) x 10^{-4}	1.32 (0.19) x 10^{-10}	
			Protein L	8.17 (1.36) x 10^5	7.13 (0.44) x 10^{-4}	8.89 (1.55) x 10^{-10}	

(version 4.2.14, Sapidyne Instruments) using a 1:1 binding equilibrium model and choosing the "unknown antigen" algorithm. The "drift correction" option was used where appropriate.

The k_a of the hmAb-Ag or hFab-Ag interactions was measured using the "direct method" as described previously [14,15]. Briefly, fixed concentration of CBP (hmAb or hFab) was mixed with the Ag concentration that bound approximately 80% of the CBP in the equilibrium experiments and the concentration of free CBP present in the sample was repeatedly measured over time using the Ag coated Azlactone beads; identical to the KinExA equilibrium assays. At least four independent experiments were performed and the resulting exponential curve of unbound hmAb or hFab as a function of time from each experiment was fit in the KinExA software to calculate the k_a of hmAb-Ag or hFab-Ag interactions. The k_d value was later determined by multiplying the k_a value measured from each experiment with the K_D value generated from the n-curve analysis.

2.3. Binding kinetics studies performed on biacore

All studies were performed using a CM5 sensor chip in freshly prepared, filtered and degassed HBS-ET buffer at 25°C. Different capture molecules were immobilized using the standard EDC/NHS chemistry reported previously [5]. In brief, the CM5 sensor surface was first activated by injecting a 1:1 (v/v) mixture of 400 mM EDC and 100 mM NHS for 10 min. Different capture reagents (20 μg/mL) prepared in 10 mM sodium acetate buffer were later injected for 6 min followed by 6 min injection of 1 M ethanolamine, pH 8.0. Supplementary Table 1 provides additional details of the immobilization conditions.

The kinetics of hmAbs binding to their respective Ag was determined on a Biacore 4000 biosensor. A similar level of hmAb was first captured over four AHC and four AHG immobilized capture surfaces. Unless specified otherwise, all capture kinetics assays were designed to have a wait time of 90 s after the capture step to ensure stabilization of the captured hmAb. Four or five Ag concentrations (serially diluted by three-fold in HBS-ET buffer) were later injected for 3 min at a flow rate of 30 μL/min followed by a dissociation phase of 1 h. At the end of each cycle, the hmAb captured over different AHC and AHG immobilized sensor surfaces were regenerated using different regeneration conditions as provided in Supplementary Table 1.

The binding of hFab to Protein A, Protein G, and Protein A/G surfaces was tested on a Biacore 3000 biosensor. The CM5 sensor surface was first immobilized with Protein A, Protein G, and Protein A/G using EDC/NHS chemistry as mentioned before. Different concentrations of hFab (3.7–900 nM, three-fold serial dilution) were injected for 30 s followed by a dissociation phase of 150 s.

The kinetics of AHC capture antibodies binding to different hmAbs was performed on a Biacore 8k biosensor by capturing the AHC capture antibody over a CM5 sensor surface immobilized with either a rabbit anti-mouse Fc antibody (GE Healthcare, Catalog# BR100838) or a mouse anti-goat Fc mAb (Southern Biotech, Catalog# 6158-01). Different concentrations of hmAbs were later injected for 30 s at a flow rate of 30 μL/min followed by a 15 min dissociation phase. Finally, the capture surfaces were regenerated as provided in Supplementary Table 1.

The Biacore 4000 and Biacore 8k binding data were first processed using Biacore 4000 and Biacore 8k evaluation software, respectively by aligning the raw data to the start of the analyte injection followed by the single reference subtraction to compensate for the changes in the refractive index. Processed data were later exported as text files and analyzed using the Scrubber software (version 2.0c, BioLogic Software, Campbell, Australia) as reported previously [5]. The Biacore 3000 data were analyzed using the Scrubber software.

3. Results

3.1. Solution based binding equilibrium measurements using KinExA

The k_a, k_d, and K_D values for the six hmAb-Ag interactions were first determined by KinExA. The binding of monovalent hFabs to their respective Ags was also characterized and their binding kinetics values were compared with those measured for bivalent hmAbs. Three-titration curves were generated to characterize each interaction by preparing samples containing three fixed concentrations of hmAb or hFab (CBP) with varying 12-16 point concentrations of serially diluted Ag. Details of the concentrations of CBP and Ag used in the KinExA are provided in Supplementary Table 2. Fig. 1 provides the three-titration curve binding equilibrium KinExA data for six hmAbs and hFabs along with the representative KinExA data for the k_a determination using the "direct method". The results of KinExA with 95% confidence interval are provided in Table 2.

All six hmAbs and hFabs bound to their respective Ag with binding affinities ranging from 3 to 22pM; hmAb-5 bound with the highest affinity (K_D = 3pM) while hmAb-4 exhibited the weakest affinity (K_D = 22pM). Both hmAbs and hFabs exhibited comparable binding affinities and percent Ag activity. With the exception of Ag-4 which showed 41% binding activity, the remaining five Ags exhibited binding activity of approximately 77–100%. During the k_a measurement, the percent Ag activity generated using the n-curve analysis was used to prepare appropriate Ag concentrations. The hmAb-5 bound with the fastest association rate ($k_a = 2.57 \times 10^7\ M^{-1}s^{-1}$), while hmAb-1 exhibited the slowest dissociation rate ($k_d = 5.37 \times 10^{-6}\ s^{-1}$).

3.2. SPR based capture kinetics analysis of six hmAbs using four anti-human IgG (AHG) and four anti-human Fc (AHC) immobilized surfaces

The kinetics of all six hmAbs binding to their respective Ags were next examined by capturing them using four AHC and four AHG capture surfaces on a Biacore 4000 biosensor. Before the immobilization, a variety of pH conditions were screened for optimal pre-concentration of the AHC and AHG capture molecules. We found that 10 mM sodium acetate buffer, pH 5.0 was best suited for the four AHC antibodies and Protein A, while 10 mM sodium acetate buffer, pH 4.0 was preferred for the pre-concentration of Protein A/G, Protein G, and Protein L. The AHC and AHG capture molecules were later individually immobilized across different flow cells on neighboring spots; either on spots 1 and 2 or on spots 4 and 5 (2 capture surfaces per flow cell) using standard amine coupling. Approximately 12,000–14,000 RU was typically observed for the immobilized AHC antibodies, while ~2,000 RU was observed for immobilized Protein A and Protein A/G. Protein L and Protein G were immobilized at ~5,000 RU and ~600 RU, respectively. Protein G was immobilized at the lowest levels amongst all four AHG capture molecules and increasing the Protein G concentration to 100 μg/mL (in 10 mM sodium acetate, pH 4.0, 4.5, or 5.0) yielded similar immobilization levels (data not shown). Despite such low immobilization levels, the Protein G surface was able to capture ~400 RU of mAb with an excellent baseline stability.

The hmAb capture levels varied between the AHC and AHG capture surfaces, with the Protein A/G surface capturing the highest level of hmAb. Between the four AHC capture antibodies, all three goat AHC pAbs captured similar levels of hmAb, while the mouse AHC mAb captured ~4-5-fold higher levels. The Protein A and Protein L surfaces captured similar levels of hmAb, which were ~1.4-fold lower than the Protein A/G surface. The Protein G surface captured ~2-fold lower levels of hmAb compared to the Protein A/G surface. With the exception of the Protein L surface, all six hmAbs captured over different AHC and AHG sensor surfaces showed excellent baseline stability with no loss in hmAb capture levels even after 1 h (data not shown); an important trait of a good capture surface. Poor baseline stability of hmAb-1, hmAb-3, and hmAb-4 was observed on the Protein L surface and,

consequently, we were unable to measure the Ag binding kinetics for these hmAbs. Regeneration conditions for different AHC and AHG surfaces were also optimized (details are provided in Supplementary Table 1). After optimization of the regeneration conditions, the sensor chip was discarded and a new CM5 sensor surface was immobilized with different capture molecules.

Picomolar affinity mAbs typically exhibit fast association and/or slow dissociation rates. Two major challenges are routinely encountered when characterizing such high affinity interactions using label-free optical biosensors – (i) Ag binding is limited by mass transport; a phenomenon referred to as mass transport limitation (MTL), which can be avoided by reducing mAb surface density [4], and (ii) reliable measurement of the k_d value for slow dissociating interactions, which requires longer dissociation times. Therefore, test experiments were first performed using all eight AHC and AHG capture surfaces and hmAb capture density, Ag concentration range, and association and dissociation times were optimized before running extensive binding kinetics studies (data not shown). We found that higher Ag concentrations were required for hmAb-2, hmAb-3, and hmAb-5 captured on Protein A and Protein A/G surfaces. We also observed that 1 h of dissociation time was required to observe at least a 5% reduction in the binding response for hmAb-1, hmAb-3, and hmAb-4. Once all the experimental conditions were established, binding studies were performed by capturing similar levels of hmAbs over different AHC and AHG capture surfaces and varying Ag concentrations were injected for 3 min.

The average kinetics values measured from three independent experiments (±standard deviation) are provided in Table 2 while the representative binding sensorgrams along with the fits generated by globally fitting the real-time binding sensorgrams using 1:1 binding model with mass transport limitation are shown in Fig. 2. The k_a values measured using SPR were found to be lower than those determined by KinExA, while both the k_d and K_D values were higher for the SPR data. For ease of comparison of the k_a, k_d, and K_D values of the six hmAb-Ag interactions characterized using eight different capture surfaces on SPR (a total of 48 different values) with the KinExA data, we calculated a fold difference in the k_a, k_d, and K_D values between the SPR and KinExA biosensors and reported as a scatter plot (Fig. 3). In comparison to the AHG capture surfaces included in the study, the AHC antibody surfaces showed a better concordance with the KinExA data, especially the three goat AHC pAb surfaces which measured only a 3-7-fold weaker binding affinities. In contrast, Protein A, Protein G, Protein A/G and Protein L surfaces were found to be non-ideal, measuring Ag binding affinities that were up to 32, 489, 2826, and 219-fold weaker, respectively, than those measured by KinExA.

Amongst the four AHG surfaces, kinetics studies performed using the Protein G surface showed the least amount of variability in the k_a, k_d, and K_D values. The differences in the k_a values measured between the Protein G surface and KinExA were less than six-fold for all six hmAbs, while the k_d values showed less than a 10-fold difference. However, this still resulted in 11-32-fold difference in the calculated K_D values. Binding studies performed on the Protein A surface yielded at least a nine-fold difference in the k_a values measured for hmAb-2, hmAb-3, hmAb-5 and hmAb-6; while at least a 14-fold faster dissociation rates of Ag-1, Ag-3 and Ag-5 were observed. In comparison to the KinExA data, a 36-fold, 58-fold, 364-fold, and 489-fold weaker binding affinity was measured for hmAb-1, hmAb-2, hmAb-3, and hmAb-5, respectively; while approximately 12-fold weaker binding affinities were determined for hmAb-4 and hmAb-6. For the Protein A/G surface, a 57-fold, 50-fold, 34-fold, and 15-fold slower k_a was measured for hmAb-2, hmAb-3, hmAb-5, hmAb-6, respectively while a 12-fold, 6-fold and 84-fold faster dissociation of Ag-1, Ag-4 and Ag-5 was observed, respectively. Interestingly, although Protein A/G is recombinantly expressed as a fusion protein of Protein A and Protein G, the Protein A/G surface yielded only a three-fold faster dissociation of Ag-3 as opposed to the 10-fold and 14-fold differences observed on Protein G and Protein A surfaces, respectively. The capture kinetics analysis performed using the Protein A/G surface generated a 38-fold, 162-fold, 138-fold, and

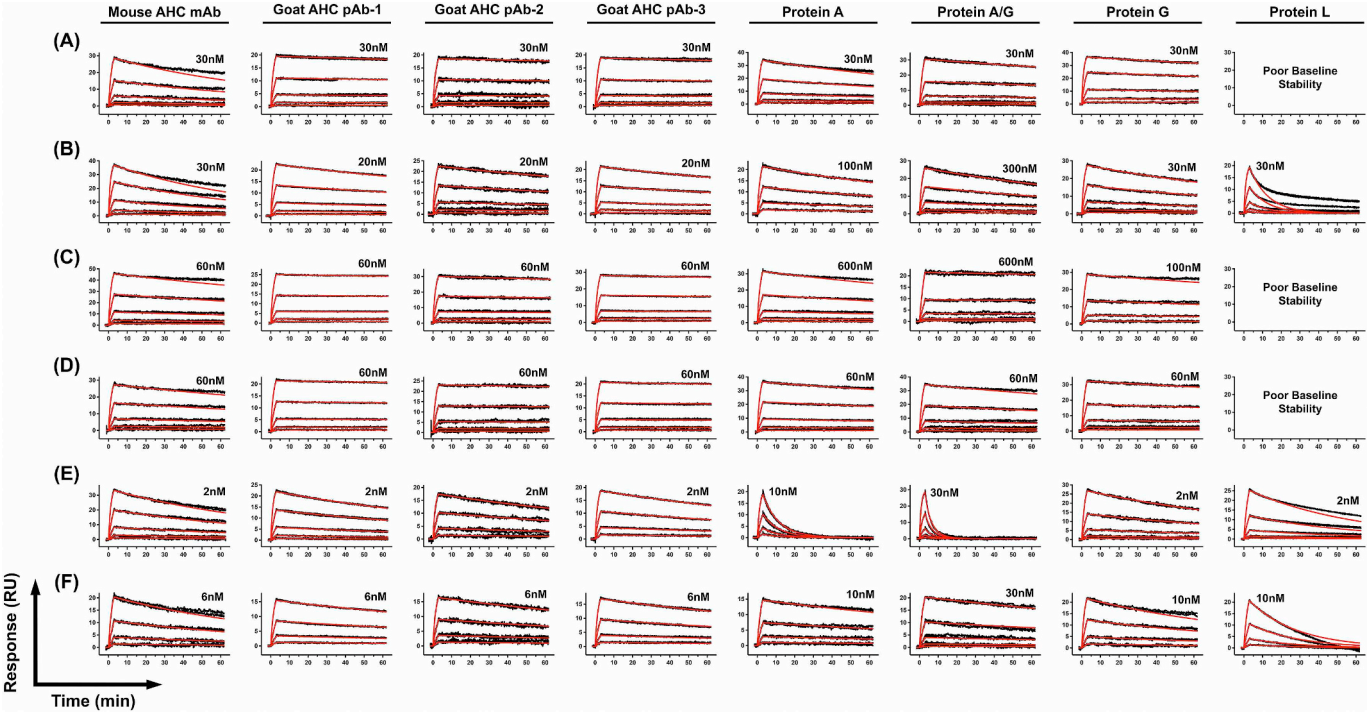

Fig. 2. Capture kinetics analysis of six hmAbs using four AHC and four AHG capture surfaces. Similar levels of (A) hmAb-1, (B) hmAb-2, (C) hmAb-3, (D) hmAb-4, (E) hmAb-5, and (F) hmAb-6 were captured over four AHC and four AHG immobilized sensor surfaces followed by injection of different concentrations of their respective Ags (serially diluted by three-fold). The real-time binding sensorgrams (shown in black) represent duplicate injections for each Ag concentration while the fits generated by globally fitting the data using a 1:1 binding model with mass transport limitation is shown as red lines. The highest concentration used to fit the real time binding sensorgrams is also provided.

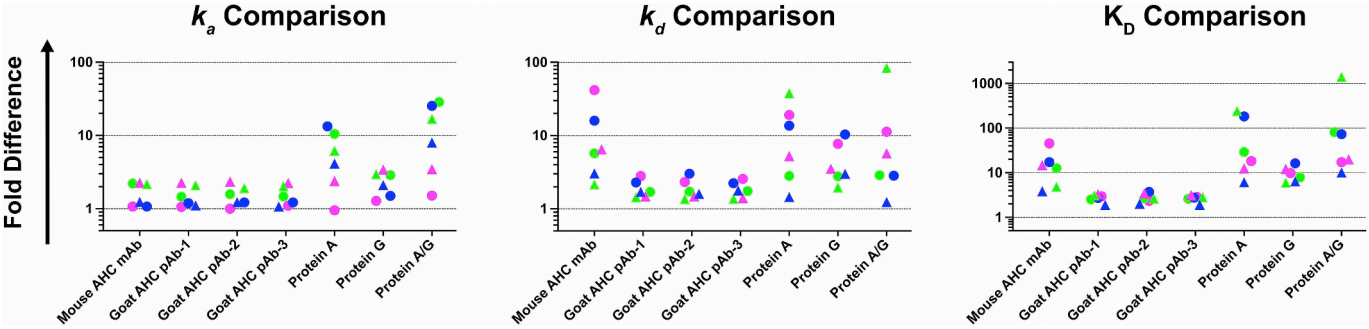

Fig. 3. Comparison of hmAb binding kinetics values generated using SPR capture kinetics and KinExA: Scatterplots show the fold difference between k_a, k_d, and K_D values of hmAb-Ag interactions generated on KinExA and on Biacore using four AHC and three AHG capture surfaces for hmAb-1 (●), hmAb-2 (●), hmAb-3 (●), hmAb-4 (▲), hmAb-5 (▲), and hmAb-6 (▲).

2826-fold weaker binding affinity for hmAb-1, hmAb-2, hmAb-3, and hmAb-5, respectively while a 20-fold weaker binding affinities were determined for hmAb-4 and hmAb-6.

Protein L was found to be the least reliable surface for capture kinetics analysis of hmAbs. Due to the poor baseline stability observed for hmAb-1, hmAb-3, and hmAb-4, binding kinetics studies could only be performed on hmAb-2, hmAb-5 and hmAb-6 using the Protein L surface. The k_a values measured for these three hmAb-Ag interactions were less than eight-fold lower in comparison to the KinExA values, but the dissociation of Ag-2 and Ag-6 were 37-fold and 15-fold faster, respectively. As a result, the calculated binding affinities measured for hmAb-2, hmAb-5 and hmAb-6 were 219-fold, 30-fold and 75-fold weaker, respectively than the affinities measured by KinExA.

The results of the kinetics analysis performed using the three goat AHC pAb surfaces were comparable and the binding kinetics values were within two-fold of each other. Furthermore, a majority of the k_a, k_d, and K_D values determined on the SPR biosensor using the three goat AHC pAbs were within six-fold of the KinExA data. The k_a values generated using the three goat AHC pAb surfaces, as well as the mouse AHC mAb surface, were only 2-4-fold lower than those measured by KinExA. The dissociation of Ags from the hmAbs captured over the three goat AHC pAb surfaces was observed to be monophasic. However, all six hmAbs captured on the mouse AHC mAb surface showed a biphasic Ag dissociation, so the first 10-30 min of the dissociation curve was used to fit the data. As a result, there was a stark difference in the k_d values measured using the three goat AHC pAb surfaces compared with those measured using the mouse AHC mAb surface. This was especially true for Ag-1 and Ag-3, which showed 37-fold and 16-fold faster dissociation rates, respectively. Moreover, in comparison to the KinExA data, the binding affinities for hmAb-1, hmAb-2, hmAb-3, and hmAb-4 measured using the mouse AHC mAb surface were 81-fold, 25-fold, 34-fold, and 15-fold weaker, respectively. Upon comparing the binding kinetics parameters measured using the four AHC antibody surfaces, we found that the k_a values for all six hmAb-Ag interactions and both k_d and K_D values for Ag-5 and Ag-6 binding to hmAb-5 and mAb-6, respectively were within two-fold of each other. However, a 13-15-fold, 3-4-fold, 5-8-fold and 4-5-fold slower dissociation rates were determined using the mouse AHC mAb surface for hmAb-1, hmAb-2, hmAb-3, and hmAb-4 respectively; resulting in a similar fold weaker binding affinities measured on the mouse AHC mAb surface.

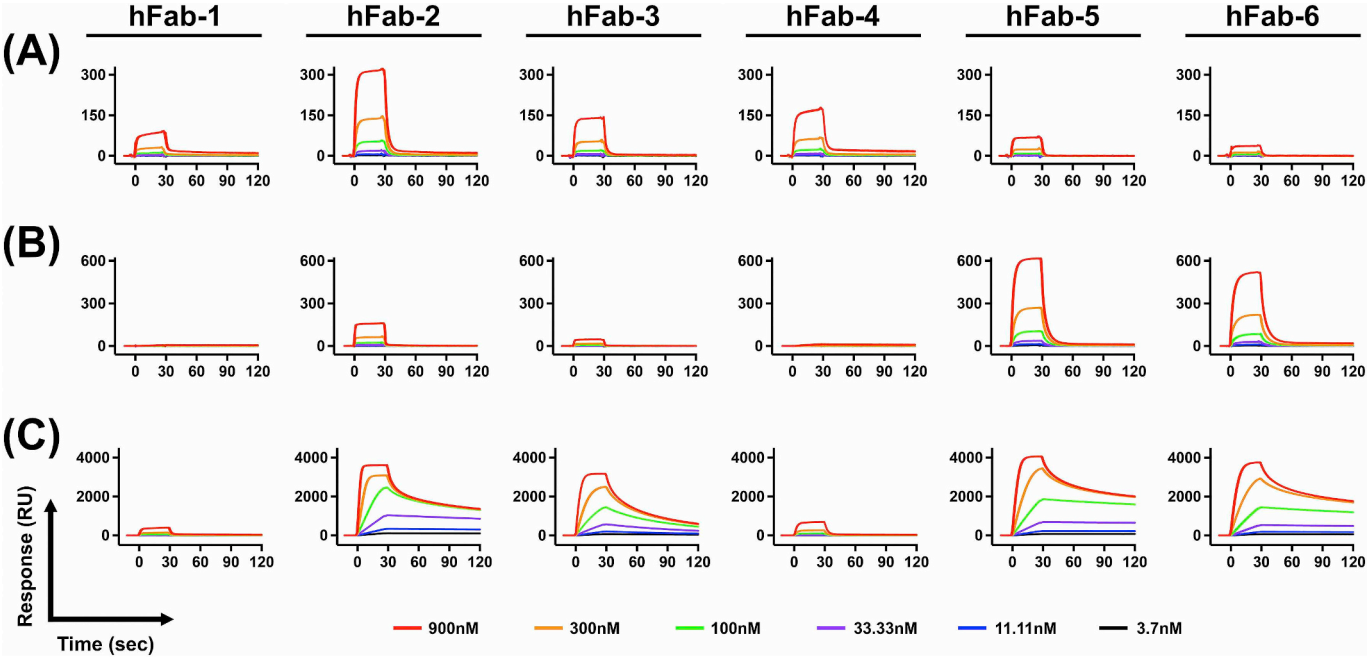

Fig. 4. Binding of hFab to Protein A, Protein G and Protein A/G surfaces. Binding of six hFabs to Protein G (A), Protein A (B), and Protein A/G (C) immobilized surfaces was studied on Biacore 3000 biosensor. Different concentrations of hFabs (serially diluted by three-fold) were injected over three AHG surfaces for 30 s followed by 150 s of dissociation. The binding sensorgrams represent duplicate injections for each concentration of hFab.

3.3. Protein A, protein G and protein A/G bind to the Fab regions of hmAbs

It is known that Protein A binds to the framework of the VH region of certain VH3 family of human IgGs [16,17], while Protein G interacts with the first β-strand in the CH1 domain of all human IgG subclasses [18]. Because both hmAb-3 and hmAb-5 utilizes the germline-encoded VH3 framework, we hypothesized that binding of Protein A and Protein A/G to the Fab region of these antibodies may impair Ag binding through steric hindrance or other mechanisms. To test this hypothesis, Fab fragments of the six hmAbs were generated and their binding to Protein A, Protein G and Protein A/G immobilized sensor surfaces were examined on a Biacore 3000 biosensor. Different concentrations of hFabs (3.7-900 nM, three-fold serial dilution) were injected in duplicate over the sensor surfaces for 30 s and double reference subtracted binding sensorgrams are shown in Fig. 4.

No detectable binding to Protein A surface was observed for hFab-1 and hFab-4, while hFab-5 and hFab-6 showed the highest binding response, followed by hFab-2 and hFab-3 (Fig. 4B). Although hmAb-4 utilizes VH3 germline framework, its Fab (hFab-4) did not bind to the Protein A surface (Fig. 4B). This is in agreement with the existing literature reporting that Protein A does not bind all Fabs that use the VH3 germline framework [17,19]. Interestingly, Ag-4 binding to hmAb-4 showed the least discrepancy in binding affinity (12-fold weaker) amongst all the hmAbs characterized using the Protein A surface, supporting our hypothesis. Further, binding of hFab-2, hFab-3, and hFab-5 to Protein A surface correlated with the 58-fold, 364-fold, and 489-fold weaker Ag binding affinities to the respective hmAbs captured on the Protein A surface. In contrast, although hFab-6 bound to the Protein A surface to similar extent as hFab-5, the Ag binding affinity measured for hmAb-6 using the Protein A surface was only 13-fold weaker compared to the KinExA data (as opposed to 489-fold weaker affinity for hmAb-5). No correlation was observed between the lack of binding of hFab-1 to the Protein A surface and the 36-fold weaker affinity for hmAb-1 measured on the Protein A surface. These data suggest that interaction of Protein A with the Fab region of hmAbs is not sufficient to explain the discrepancy in the binding affinities of hmAb-Ag interactions that were measured by SPR using a Protein A surface with those measured by KinExA.

As anticipated, all six hFabs bound to the Protein G surface, but the extent of binding varied between the hFabs. The highest binding signal was observed for hFab-2, while hFab-6 bound with the lowest binding response (Fig. 4A). Interestingly, the human IgG4 subclass (hFab-1, hFab5, and hFab-6) showed lower binding responses compared to the human IgG1 subclass (hFab-2, hFab-3, and hFab-4), suggesting that Protein G may bind the CH1 domain of human IgG4 with a weaker affinity than IgG1. It is important to note that in comparison to the Protein A and Protein A/G surfaces, capture kinetics analysis performed on the Protein G surface showed a better correlation with the KinExA data. However, our data showed no correlation between hFab binding to Protein G and the observed discrepancy in the K_D values generated using capture kinetics analysis on Protein G surface (Table 2). All K_D values measured with Protein G were within 20-fold of the KinExA values, with the exception of hmAb-3. These data suggest that Protein G binding to the Fab may not significantly interfere Ag binding, as was observed for the Protein A capture surface.

Higher binding of hFab was observed to the Protein A/G surface compared to the Protein A and Protein G surfaces (Fig. 4C). Protein A/G is recombinantly expressed as a fusion of Protein A and Protein G and it was interesting to observe the enhanced binding only for those hFabs that bound to both Protein A and Protein G surfaces (hFab-2, hFab-3, hFab-5 and hFab-6). This suggests that hFabs can simultaneously bind to the Protein A binding epitope (framework of the VH region) and to the Protein G binding epitope (CH1 domain) present on the Protein A/G molecule, resulting in a cooperative binding with increased binding affinity. This cooperative binding is expected to occur through the hFab binding either to the same or to a neighboring Protein A/G molecule, owing to the high-density of immobilized Protein A/G on the surface. Since no detectable binding was observed for hFab-1 or hFab-4 on the Protein A surface, lower binding responses were detected for these hFabs on the Protein A/G surface. Interestingly, there was a strong correlation between enhanced surface binding of hFabs and the fold difference in the Ag binding affinities measured for hmAbs captured using the Protein A/G surface. The Ag binding kinetics analysis performed using Protein A/G surface for three of the four hmAbs whose hFabs showed enhanced binding to Protein A/G surface (hmAb-2, hmAb-3, and hmAb-5) were 162-fold, 138-fold, and 2826-fold weaker,

Table 3
Kinetics of four AHC antibodies binding to six hmAbs at two densities.

		~8RU Capture Density				~200RU Capture Density			
hmAb	AHC Antibody Captured	k_a (1/Ms)	k_d (1/s)	K_D (M)	t½ (min)	k_a (1/Ms)	k_d (1/s)	K_D (M)	t½ (min)
hmAb-1	Mouse AHC mAb	4.71×10^5	4.16×10^{-3}	8.89×10^{-9}	2.8	4.70×10^5	4.87×10^{-3}	1.04×10^{-8}	2.4
	Goat AHC pAb-1	1.56×10^6	6.58×10^{-4}	4.21×10^{-10}	17.6	1.55×10^6	1.35×10^{-4}	8.66×10^{-11}	85.6
	Goat AHC pAb-2	1.64×10^6	1.87×10^{-3}	1.14×10^{-9}	6.2	1.49×10^6	4.94×10^{-4}	3.31×10^{-10}	23.4
	Goat AHC pAb-3	1.43×10^6	3.80×10^{-4}	2.66×10^{-10}	30.4	1.28×10^6	9.96×10^{-5}	7.76×10^{-11}	116.0
hmAb-2	Mouse AHC mAb	8.21×10^5	5.02×10^{-3}	6.12×10^{-9}	2.3	7.20×10^5	5.59×10^{-3}	7.77×10^{-9}	2.1
	Goat AHC pAb-1	1.77×10^6	2.98×10^{-4}	1.68×10^{-10}	38.8	1.97×10^6	9.98×10^{-5}	5.06×10^{-11}	115.7
	Goat AHC pAb-2	1.73×10^6	4.28×10^{-4}	2.47×10^{-10}	27.0	1.76×10^6	1.21×10^{-4}	6.87×10^{-11}	95.5
	Goat AHC pAb-3	1.55×10^6	1.42×10^{-4}	9.16×10^{-11}	81.3	1.67×10^6	4.51×10^{-5}	2.70×10^{-11}	256.1
hmAb-3	Mouse AHC mAb	6.37×10^5	3.49×10^{-3}	5.49×10^{-9}	3.3	5.66×10^5	4.25×10^{-3}	7.50×10^{-9}	2.7
	Goat AHC pAb-1	1.37×10^6	3.48×10^{-4}	2.55×10^{-10}	33.2	1.60×10^6	9.01×10^{-5}	5.63×10^{-11}	128.2
	Goat AHC pAb-2	1.26×10^6	3.84×10^{-4}	3.06×10^{-10}	30.1	1.46×10^6	1.13×10^{-4}	7.74×10^{-11}	102.2
	Goat AHC pAb-3	1.23×10^6	2.10×10^{-4}	1.71×10^{-10}	55.0	1.41×10^6	4.85×10^{-5}	3.43×10^{-11}	238.1
hmAb-4	Mouse AHC mAb	4.62×10^5	4.17×10^{-3}	9.03×10^{-9}	2.8	4.87×10^5	4.68×10^{-3}	9.60×10^{-9}	2.5
	Goat AHC pAb-1	1.19×10^6	2.81×10^{-4}	2.36×10^{-10}	41.1	1.50×10^6	9.11×10^{-5}	6.09×10^{-11}	126.8
	Goat AHC pAb-2	1.23×10^6	3.98×10^{-4}	3.23×10^{-10}	29.0	1.36×10^6	1.34×10^{-4}	9.88×10^{-11}	86.2
	Goat AHC pAb-3	1.32×10^6	1.05×10^{-4}	7.98×10^{-11}	110.0	1.31×10^6	4.74×10^{-5}	3.63×10^{-11}	243.7
hmAb-5	Mouse AHC mAb	2.30×10^5	8.35×10^{-3}	3.63×10^{-8}	1.4	3.45×10^5	8.38×10^{-3}	2.43×10^{-8}	1.4
	Goat AHC pAb-1	1.11×10^6	9.10×10^{-5}	8.24×10^{-11}	126.9	1.08×10^6	6.80×10^{-5}	6.29×10^{-11}	169.9
	Goat AHC pAb-2	1.36×10^6	1.97×10^{-4}	1.44×10^{-10}	58.6	1.04×10^6	1.28×10^{-4}	1.22×10^{-10}	90.2
	Goat AHC pAb-3	1.18×10^6	6.21×10^{-5}	5.28×10^{-11}	186.0	8.81×10^5	3.43×10^{-5}	3.89×10^{-11}	336.7
hmAb-6	Mouse AHC mAb	2.68×10^5	8.51×10^{-3}	3.18×10^{-8}	1.4	4.11×10^5	8.44×10^{-3}	2.06×10^{-8}	1.4
	Goat AHC pAb-1	1.22×10^6	6.15×10^{-4}	5.06×10^{-10}	18.8	1.34×10^6	2.64×10^{-4}	1.97×10^{-10}	43.8
	Goat AHC pAb-2	1.42×10^6	2.09×10^{-3}	1.49×10^{-9}	5.5	1.25×10^6	9.85×10^{-4}	7.90×10^{-10}	11.7
	Goat AHC pAb-3	1.17×10^6	7.53×10^{-4}	6.46×10^{-10}	15.3	1.10×10^6	1.94×10^{-4}	1.76×10^{-10}	59.5

respectively. These data support our theory that binding of hFabs to Protein A and Protein A/G surfaces may impair Ag binding through steric hindrance or other mechanisms.

3.4. Mouse AHC mAb binds hmAbs with weak affinity, but the three goat AHC pAbs have high affinity to hmAbs with slow dissociation rate constant

An important requirement for performing capture kinetics analysis using a label-free biosensor is that the tag-specific capture molecule forms a stable complex with the captured ligand and has a minimal to no drop in the capture level over the course of the experiment. Once immobilized on the CM5 Biacore sensor surface at high density, all four AHC capture antibodies included in this study showed excellent baseline stability even at a 500 RU capture level of hmAb (data shown). Therefore, the observed discrepancy in the binding kinetics values generated using the mouse AHC mAb could not be explained based on the instability of the captured hmAb. We had previously observed that the stability of the captured human IgG depended on the immobilization level of the mouse AHC mAb. Poor baseline stability of captured human IgG was typically observed for immobilization densities of less than 1000 RU and therefore, we usually aim to immobilize greater than 3000 RU of mouse AHC mAb for our capture kinetics analyses. However, such high immobilization levels were not required for the goat AHC pAb-1 to stably capture hmAbs (data not shown). In light of this observation, we thought that the affinity of mouse AHC mAb binding to human IgG may be weak. We therefore investigated the true 1:1 binding affinity of all four AHC antibodies included in this study. Because the Fc region of IgG is a dimer, the values measured for AHC antibodies binding to the Fc region could be influenced by the bivalency of the human IgG. To reduce potential avidity effects caused by the bivalent analyte (human IgG), binding kinetics studies were performed using a low-density (~8RU) AHC antibody surface. Moreover, to

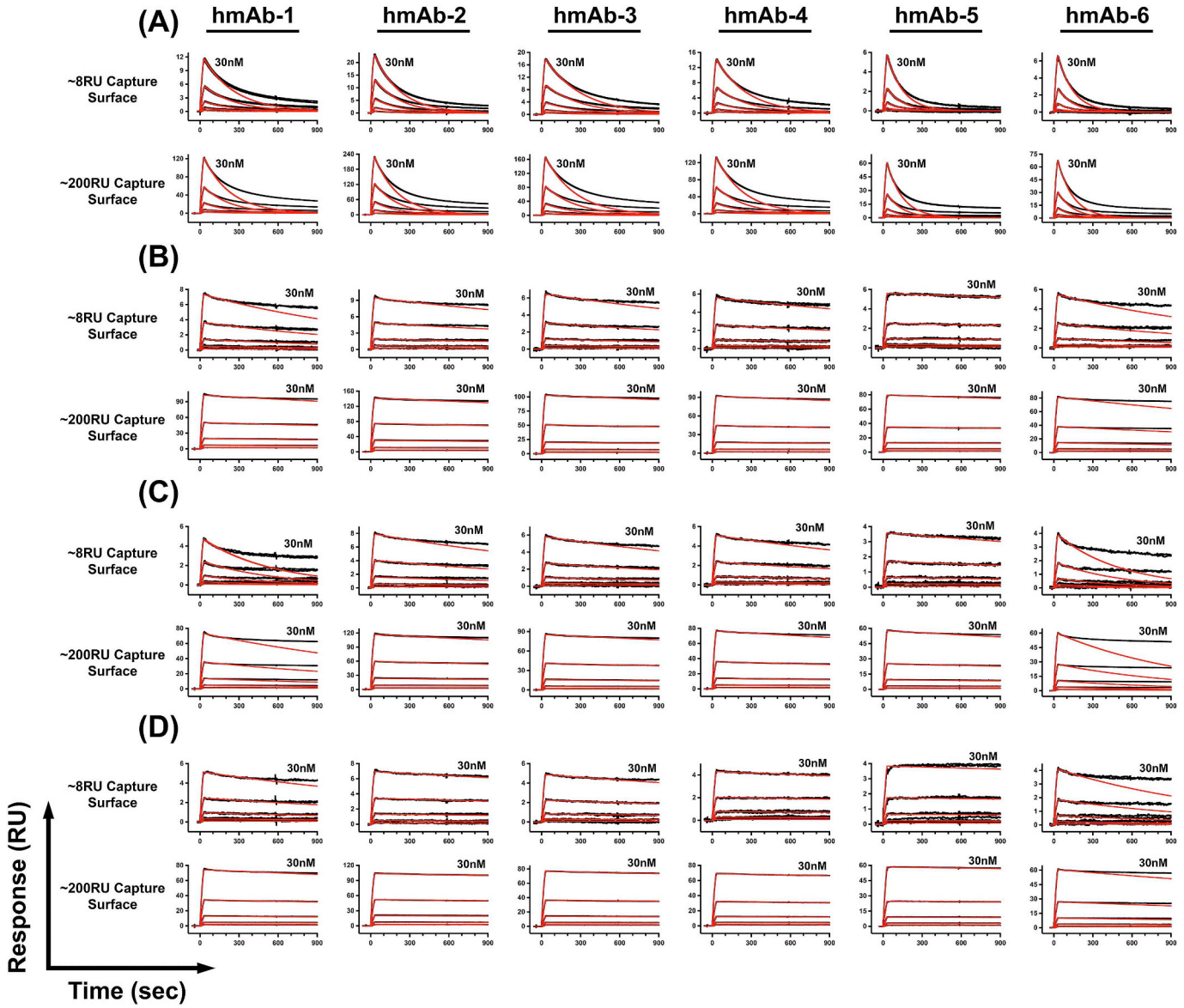

Fig. 5. Capture kinetics analysis of four AHC antibodies binding to six hmAbs. Kinetics of four AHC capture antibodies binding to six hmAbs was performed on Biacore 8k biosensor. Binding studies were performed by capturing 8RU or 200RU surface densities of mouse AHC mAb or goat AHC pAb on a CM5 sensor surface immobilized with rabbit anti-mouse Fc pAb or mouse anti-goat Fc mAb, respectively. Different concentrations of hmAbs (serially diluted by three-fold) were injected over (A) mouse AHC mAb, (B) goat AHC pAb-1, (C) goat AHC pAb-2, and (D) goat AHC pAb-3 captured surfaces for 30 s followed by 15 min of dissociation phase. The real-time binding sensorgrams are shown in black while red lines represent fits generated using 1:1 binding model with mass transport limitation. The binding sensorgrams represent duplicate injections of each hmAb concentration and the highest concentration used to fit the data is reported.

understand the role of AHC antibody surface density on the kinetics of hmAb binding, kinetics studies were also performed with a 200 RU AHC antibody surface. The mouse AHC mAb or goat AHC pAbs were captured using a rabbit anti-mouse Fc pAb and mouse anti-goat Fc mAb immobilized sensor surfaces, respectively. The results of the kinetics analysis are provided in Table 3 and the representative real-time binding sensorgrams are shown in Fig. 5.

Biphasic dissociation was observed for all four AHC antibodies captured at 8 RU and the initial 1-2 min of the dissociation phase was used to fit the data. All three goat AHC pAbs bound hmAbs with high affinity (82pM-1.5 nM) and $t_{½}$ values ranged from 5.5 to 186 min. Increasing the surface density to 200 RU further increased the binding affinities by up to five-fold. The k_a values were comparable between the two surface densities, but slower dissociation rates were observed on the 200 RU surface with the $t_{½}$ values ranging from 44 to 337 min. This is consistent with the avidity effects associated with the binding of bivalent hmAbs to a high density of captured AHC antibodies. The goat AHC pAb-2 showed a 2-3-fold faster dissociation of hmAb compared to goat AHC pAb-1 and pAb-3 for both surface densities. In contrast, mouse AHC mAb bound to all six hmAbs with significantly weaker affinity with $t_{½}$ values ranging from 1.4 to 3.3 min. Surprisingly, increasing the capture density of mouse AHC mAb to 200 RU did not significantly reduce the dissociation rate of hmAbs, as was observed for the three goat AHC pAbs, and the $t_{½}$ values were observed to be comparable to the 8 RU surface. For both mouse AHC mAb capture densities, 2-3-fold faster dissociation rates were measured for hmAb-5 and hmAb-6 resulting in a comparable fold difference in their K_D values.

4. Discussion

In this study, we showcased that the selection of the capture molecule used to perform capture kinetics analysis of hmAb-Ag interaction on label-free optical biosensor can have a profound effect on the accuracy of the measured k_a, k_d and K_D values. To demonstrate this, we characterized six picomolar affinity hmAb-Ag interactions using four AHC capture surfaces (mouse AHC mAb, and three goat AHC pAbs) and four AHG capture surfaces (Protein A, Protein G, Protein A/G and Protein L). Based on the solution based binding equilibrium affinity measured on a KinExA 3200 biosensor, all six hmAbs bound to their respective Ag with the K_D values ranging from 3 to 22 pM. Both hmAbs and hFabs bound to their respective Ag with less than two-fold difference in the k_a, k_d and K_D values, suggesting that the bivalency of hmAbs did not affect the Ag binding in KinExA.

We later performed capture kinetics analysis on different capture surfaces and discovered large discrepancies between the SPR data generated using Protein A, Protein G, Protein A/G, Protein L and mouse AHC mAb immobilized surfaces and the KinExA data. The Protein L surface was the worst of the four AHG capture surfaces used in this study. The binding affinities measured for four hmAbs (hmAb-1, hmAb-2, hmAb-3, and hmAb-5) using Protein A and Protein A/G surfaces were at least 36-fold weaker than those measured by KinExA (Supplementary Table 3). We hypothesized that binding of Protein A and Protein G to the Fab region of human IgG may influence Ag binding due to steric hindrance or other mechanism. Clearly, the observed correlation between hFab-2, hFab-3, and hFab-5 binding to Protein A and the fold weaker Ag binding affinity to their respective hmAbs captured on Protein A surface supported our hypothesis. Interestingly, although hFab-6 bound to Protein A and Protein A/G surfaces with binding response comparable to hFab-5, only a 13-fold and 20-fold weaker binding affinity was observed for hmAb-6 captured on Protein A and Protein A/G surfaces, respectively. We understand that factors such as the hmAb paratope and the Ag epitope plays a role in how these interactions affect hmAb-Ag binding affinities. Thus, we speculate that the paratope of hmAb-6 may be distant from the Protein A binding epitope and that Ag-6 binding might not be as sterically hindered as one would expect for Ag-5. However, additional studies would be required to support this theory, which is beyond the scope of the current embodiment. It was also surprising to discover that although hFab-1 did not interact with the Protein A surface, a 36-fold and 38-fold weaker Ag-1 binding affinity was measured for hmAb-1 captured on Protein A and Protein A/G surfaces, respectively. Clearly, the source of this discrepancy cannot be explained just based on the hFab binding to Protein A or Protein A/G surfaces, and some other mechanism is influencing the results of the capture kinetics analysis performed on these surfaces. In contrast to the Protein A and Protein A/G surfaces, smaller discrepancies in the K_D values of the hmAb-Ag interactions were observed using the Protein G surface (10-20-fold weaker). However, we were unable to find any correlation between hFab binding to the Protein G surface and the observed fold difference in the measured binding kinetics values. Based on these observations and also the uncertainty in understanding the effect of hmAb binding to Protein G, Protein A or Protein A/G surfaces on Ag binding, we would not recommend using these surfaces for performing capture kinetics analysis to characterize mAb-Ag interactions.

We understand that multiple factors such as surface charge of the reagents (ligand and analyte), biosensor surface charge, conjugation chemistry, baseline stability of captured ligand, and immobilization level of the tag-specific capture molecule can influence the results of the binding kinetics assays performed on the optical biosensors [7,20,21]. Therefore, all of our binding studies were performed under similar conditions to minimize the variability in the results; especially for the four AHC antibody surfaces. However, we still observed discrepancies in the k_d values measured using the mouse AHC mAb and the three goat AHC pAb surfaces. The most striking discrepancy was observed for hmAb-1 wherein the Ag-1 dissociated almost 37-fold faster in comparison to the k_d value calculated using KinExA. It was perplexing why the mouse AHC mAb generated inaccurate results given that the surface had a higher binding capacity than the goat AHC pAbs and also captured all six hmAbs with excellent stability even after 1 h of dissociation. Moreover, unlike Protein A, Protein G, and Protein A/G surfaces, this mAb specifically binds to the Fc region of human IgG. Therefore, the observed fold difference could not be explained based on the probable steric hindrance of Ag binding. Upon further investigation we found that once bound to the mouse AHC mAb, all hmAbs showed fast dissociation on both 8 and 200 RU surfaces with $t_{½}$ values ranging from 1.4 to 3.3 min. In contrast, all three goat AHC pAbs had sub-nanomolar binding affinities (200 RU surface) for all six hmAbs characterized in this study with $t_{½}$ values ranging from 11.7 to 337 min.

Based on the observed binding profile, we believe that the mouse AHC mAb surface relies on the rebinding of the captured human IgG to achieve a stable baseline. Such rebinding typically results in the reduction of the apparent dissociation rate and in turn will artificially show that the human IgG is stably captured on the sensor surface. It is important to understand that this rebinding phenomenon is dependent on the surface density and reducing the immobilization level impairs the rebinding of captured human IgG, observed as instable baseline with fast dissociation, as seen in the 200 RU surface (Fig. 5). It was also intriguing to find that the capture kinetics analysis performed on the mouse AHC mAb surface showed biphasic dissociation of Ag for all six hmAbs; fast dissociation for the first 10-30 min followed by slow dissociation during the last 10 min of the dissociation phase (Fig. 2). The largest biphasic profile was observed for hmAb-1 and hmAb-3 which also exhibit the slowest dissociation rate. Based on these observations we believe that the Ag binding to hmAb might interfere with the rebinding of the captured hmAb (which is critical for mouse AHC mAb surface) and as a result a small percentage of hmAb-Ag complex dissociates from the sensor surface. Since the molecular weight of hmAb-1 is almost 10-fold higher than Ag-1, one would expect a larger drop in the binding response following the dissociation of the complex, in comparison to the Ag-1 dissociation. This would reflect a faster apparent dissociation rate in the binding sensorgram, as observed for

hmAb-1 and hmAb-3. Based on the slower dissociation during the last 10 min of dissociation phase, we feel that a small fraction of the captured hmAb achieves better capture stability during the 1 h dissociation phase and the observed change in the binding response is the true dissociation of Ag. However, additional studies would be required to substantiate this theory and it is beyond the scope of this work. In light of these findings, we also characterized rabbit anti-mouse Fc pAb and mouse anti-goat Fc mAb which were used to capture mouse AHC mAb and goat AHC pAbs, respectively and confirmed that they bound with high affinity to mouse IgG and goat IgG, respectively (data not shown).

The six hmAbs included in this study were selected based on the screening of a panel of 44 high affinity hmAbs binding to 22 different molecular weight Ags - two hmAbs per Ag (data not shown). The k_a, k_d and K_D values generated using the three goat AHC pAbs were within two-fold of each other. Protein L was the worst capture surface and the K_D values measured for only 16 hmAbs were within three-fold of the values measured using the goat AHC pAb surface. Moreover, Protein L surface failed to capture three hmAbs while nine hmAbs showed poor baseline stability. Amongst the remaining four capture surfaces (mouse AHC mAb, Protein G, Protein A, and Protein A/G), the kinetics values measured using the mouse AHC mAb showed a better correlation with the data generated using goat AHC pAb. Out of 44 hmAbs, the binding affinity measured for only nine hmAbs were more than two-fold weaker than the values measured using goat AHC pAb-1 surface. In contrast, binding affinities of 7, 14, and 24 hmAbs measured using Protein G, Protein A, and Protein A/G surfaces, respectively were more than two-fold weaker than the data generated using goat AHC pAb-1. Although all seven capture surfaces (except Protein L) showed excellent baseline stability of captured hmAb, it was startling for us to discover such variability in the results of the capture kinetics analysis. We therefore selected six representative hmAbs in this study which showed largest variability in the results across different AHC and AHG capture surfaces.

The current norm in the label-free community to evaluate a tag-specific capture reagent is to first immobilize it onto the sensor surface at a high density and then test the ability of the immobilized surface to stably capture the ligand. In this study, we showed that for accurate measurement of k_a, k_d and K_D values of hmAb-Ag interactions, a high affinity capture reagent with slow dissociation rate that specifically binds to the Fc region of human IgG is essential; similar to the three goat AHC pAbs. Our data provides new insight on the selection of the capture reagent and we are hopeful that these data will motivate everyone to reconsider their traditional practice. We encourage the entire label-free community to adopt the proposed methodology for the selection of a capture reagent – (i) determine the true 1:1 kinetics of the capture reagent binding to the tag specific ligand, and (ii) immobilize the high affinity capture reagent on the sensor surface at a high density to perform capture kinetics assays on optical biosensors.

Disclosure summary

All the authors are employees and shareholders of Regeneron Pharmaceuticals.

Acknowledgements

We thank Joel Martin and his group for cloning and purifying all the recombinant proteins used in the study. We also appreciate preclinical manufacturing and process development team for purifying hmAbs and Ags included in the study. We are also thankful to our collaborators at Adimab for developing hmAb-1.

Appendix A. Supplementary data

Supplementary data to this article can be found online at https://doi.org/10.1016/j.ab.2020.113580.

References

[1] Z. Elgundi, M. Reslan, E. Cruz, V. Sifniotis, V. Kayser, The state-of-play and future of antibody therapeutics, Adv. Drug Deliv. Rev. 122 (2017) 2–19.
[2] A.J. Murphy, L.E. Macdonald, S. Stevens, M. Karow, A.T. Dore, K. Pobursky, T.T. Huang, W.T. Poueymirou, L. Esau, M. Meola, W. Mikulka, P. Krueger, J. Fairhurst, D.M. Valenzuela, N. Papadopoulos, G.D. Yancopoulos, Mice with megabase humanization of their immunoglobulin genes generate antibodies as efficiently as normal mice, Proc. Natl. Acad. Sci. U.S.A. 111 (2014) 5153–5158.
[3] L.E. Macdonald, M. Karow, S. Stevens, W. Auerbach, W.T. Poueymirou, J. Yasenchak, D. Frendewey, D.M. Valenzuela, C.C. Giallourakis, F.W. Alt, G.D. Yancopoulos, A.J. Murphy, Precise and in situ genetic humanization of 6 Mb of mouse immunoglobulin genes, Proc. Natl. Acad. Sci. U.S.A. 111 (2014) 5147–5152.
[4] V. Kamat, A. Rafique, Exploring sensitivity and throughput of a parallel flow SPRi biosensor for characterization of antibody-antigen interaction, Anal. Biochem. 525 (2017) 8–22.
[5] V. Kamat, A. Rafique, Extending the throughput of Biacore 4000 biosensor to accelerate kinetic analysis of antibody-antigen interaction, Anal. Biochem. 530 (2017) 75–86.
[6] V. Kamat, A. Rafique, Designing binding kinetic assay on the bio-layer interferometry (BLI) biosensor to characterize antibody-antigen interactions, Anal. Biochem. 536 (2017) 16–31.
[7] A.W. Drake, M.L. Tang, G.A. Papalia, G. Landes, M. Haak-Frendscho, S.L. Klakamp, Biacore surface matrix effects on the binding kinetics and affinity of an antigen/antibody complex, Anal. Biochem. 429 (2012) 58–69.
[8] C. Bee, Y.N. Abdiche, D.M. Stone, S. Collier, K.C. Lindquist, A.C. Pinkerton, J. Pons, A. Rajpal, Exploring the dynamic range of the kinetic exclusion assay in characterizing antigen-antibody interactions, PLoS One 7 (2012) e36261.
[9] N. Papadopoulos, J. Martin, Q. Ruan, A. Rafique, M.P. Rosconi, E. Shi, E.A. Pyles, G.D. Yancopoulos, N. Stahl, S.J. Wiegand, Binding and neutralization of vascular endothelial growth factor (VEGF) and related ligands by VEGF Trap, ranibizumab and bevacizumab, Angiogenesis 15 (2012) 171–185.
[10] T. Yano, H. Takeda, A. Uematsu, S. Yamanaka, S. Nomura, K. Nemoto, T. Iwasaki, H. Takahashi, T. Sawasaki, AGIA tag system based on a high affinity rabbit monoclonal antibody against human dopamine receptor D1 for protein analysis, PLoS One 11 (2016) e0156716.
[11] R.L. Rich, M.J. Cannon, J. Jenkins, P. Pandian, S. Sundaram, R. Magyar, J. Brockman, J. Lambert, D.G. Myszka, Extracting kinetic rate constants from surface plasmon resonance array systems, Anal. Biochem. 373 (2008) 112–120.
[12] D. Yang, A. Singh, H. Wu, R. Kroe-Barrett, Comparison of biosensor platforms in the evaluation of high affinity antibody-antigen binding kinetics, Anal. Biochem. 508 (2016) 78–96.
[13] R. Karlsson, E. Pol, A. Frostell, Comparison of surface plasmon resonance binding curves for characterization of protein interactions and analysis of screening data, Anal. Biochem. 502 (2016) 53–63.
[14] P. Rathanaswami, S. Roalstad, L. Roskos, Q.J. Su, S. Lackie, J. Babcook, Demonstration of an in vivo generated sub-picomolar affinity fully human monoclonal antibody to interleukin-8, Biochem. Biophys. Res. Commun. 334 (2005) 1004–1013.
[15] A.W. Drake, D.G. Myszka, S.L. Klakamp, Characterizing high-affinity antigen/antibody complexes by kinetic- and equilibrium-based methods, Anal. Biochem. 328 (2004) 35–43.
[16] P.W. Roben, A.N. Salem, G.J. Silverman, VH3 family antibodies bind domain D of staphylococcal protein A, J. Immunol. 154 (1995) 6437–6445.
[17] M. Graille, E.A. Stura, A.L. Corper, B.J. Sutton, M.J. Taussig, J.B. Charbonnier, G.J. Silverman, Crystal structure of a Staphylococcus aureus protein A domain complexed with the Fab fragment of a human IgM antibody: structural basis for recognition of B-cell receptors and superantigen activity, Proc. Natl. Acad. Sci. U. S. A. 97 (2000) 5399–5404.
[18] J.P. Derrick, D.B. Wigley, The third IgG-binding domain from streptococcal protein G. An analysis by X-ray crystallography of the structure alone and in a complex with Fab, J. Mol. Biol. 243 (1994) 906–918.
[19] E.H. Sasso, G.J. Silverman, M. Mannik, Human IgA and IgG F(ab')2 that bind to staphylococcal protein A belong to the VHIII subgroup, J. Immunol. 147 (1991) 1877–1883.
[20] Y.N. Abdiche, K.C. Lindquist, A. Pinkerton, J. Pons, A. Rajpal, Expanding the ProteOn XPR36 biosensor into a 36-ligand array expedites protein interaction analysis, Anal. Biochem. 411 (2011) 139–151.
[21] M. Katayama, T. Sato, J. Kuromitsu, Capture molecules preconditioned for kinetic analysis of high-affinity antigen-antibody complex in Biacore A100, Anal. Biochem. 424 (2012) 168–177.